Currents in Stratified Water Bodies 2: Internal Waves

L Boegman, Queen's University, Kingston, ON, Canada

Introduction

In the surface layer of lakes, exchange with the atmosphere and energetic mixing from wind and convection provides oxygen and light, thus enabling growth of plankton and other aquatic life. The nutrients required to sustain surface layer ecology are primarily found in the benthos, where sediment resuspension, nutrient release from the sediments, and oxygen consumption occur. In the interior of lakes, seasonal stratification of the water column suppresses vertical mixing, effectively isolating the surface layer from the sediments. However, the stratification simultaneously provides an ideal environment for internal waves, whose oscillatory currents energize a quasi-steady turbulent benthic boundary layer (TBBL) that drives vertical biogeochemical flux.

The wave motions in lakes are initiated by the surface wind stress. Waves will occur on both the free surface and internal stratifying layers (e.g., the thermocline) and these are referred to as surface or barotropic and internal or baroclinic motions, respectively. The waves are categorized according to their length scale. Basin-scale waves have wavelengths that are of the same order as the lake diameter and are manifest as standing wave modes – or seiches. Sub-basin-scale waves have wavelengths of 10–1000 m. These waves are progressive in nature and will break where they shoal on sloping topography at the depth of the thermocline.

Characteristic Geometry and Water-Column Stratification

The internal waves described in this chapter are in lakes that are not affected by the Coriolis force due to the Earth's rotation: for example, small lakes in the arctic, mid-sized lake (i.e., diameter $>\sim 5$ km) in the mid latitudes, and large lakes near the equator. These lakes have a Burger number >1. As we shall see later, the wave modes that are supported in such lakes depend upon the nature of the water column stratification.

We limit the analysis to several characteristic types of stratification that are commonly observed to occur. The simplest case is that of a homogenous lake of length L and depth H, as may be typical for a shallow system or one that has recently experienced a turnover event (Figure 1(a)). During the summer months, solar heating causes a lake to become stratified with a layered structure consisting of an epilimnion, metalimnion, and hypolimnion (see **The Surface Mixed Layer in Lakes and Reservoirs**). If the vertical density gradient is abrupt through the metalimnion, the lake may be approximated as a simple two-layer system of thickness h_1 and density ρ_1 over thickness h_2 and density ρ_2, where $H = h_1 + h_2$ is the total depth (Figure 1(b)). In lakes where a strong diurnal thermocline is present or the metalimnion is thick, the vertical density structure may be approximated with three contiguous fluid layers of density ρ_1, ρ_2, and ρ_3 with thicknesses $H = h_1 + h_2 + h_3$ (Figure 1(c,d)). The layered model for the stratification is inappropriate for shallow lakes ($H < \sim 15$ m), where the entire water column may be composed of weakly stratified water (e.g., western Lake Erie). In these lakes a transient diurnal thermocline may still occur. Shallow weakly stratified lakes are best characterized as having a continuous stratification (Figure 1(e)). Very deep lakes (with a thick laminar region between the metalimnion and TBBL) and those with a significant chemical (saline) component will also have a continuous stratification beneath the metalimnion (Figure 1(f)). In general, the strength of the stratification is measured according to the Brunt-Väisälä or buoyancy frequency $N = \sqrt{-(g/\rho_o)d\rho/dz}$, where z is the vertical coordinate direction, g is the gravitational constant, and $\rho_o = 1000\,\mathrm{kg\,m^{-3}}$ is the characteristic water density; in the thermocline of lakes the maximum $N \sim 10^{-2}$ Hz.

Surface Momentum Transfer and Wind Set-Up

Wind Set-Up of the Free Surface

The action of the wind across the lake surface results in frictional momentum transfer from the wind to the water (see **The Surface Mixed Layer in Lakes and Reservoirs**). This transfer occurs in the form of a stress (N m^{-2}) applied at the free surface. The stress may be parameterized as

$$\tau = C_D \rho_a U_{10}^2$$

where C_D is the drag coefficient, $\rho_a = 1.2\,\mathrm{kg\,m^{-3}}$ is the air density, and U_{10} the wind speed measured at 10 m above the water surface. Typically $C_D = 1.3 \times 10^{-3}$, but this value may vary by $\pm 40\%$ depending upon the wind speed, water depth, and relative temperature

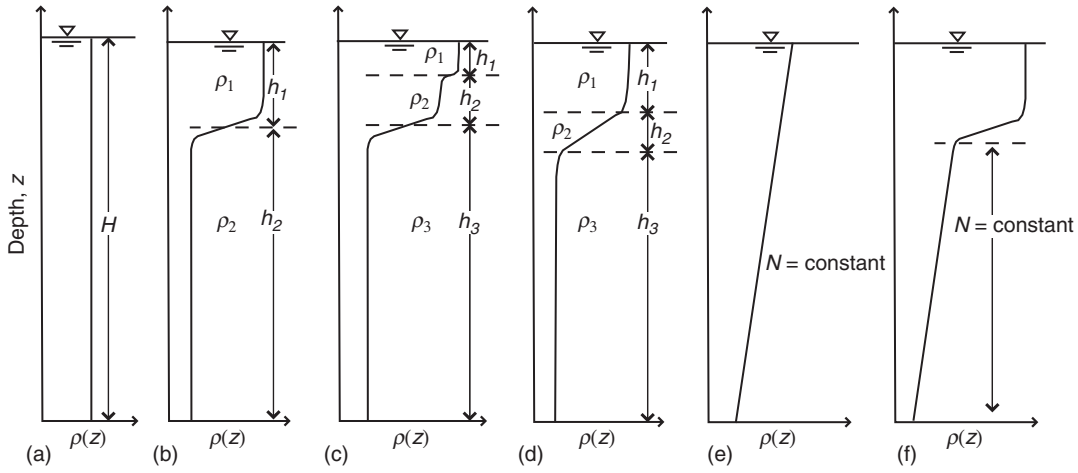

Figure 1 Characteristic continuous water-column stratifications as found in lakes and typical layer approximations. (a) Homogeneous water-column of constant density. (b) Two-layer approximation of the continuous stratification, where the layer separation occurs at the thermocline. (c) Three-layer approximation of the continuous stratification, where the layer separation occurs at the diurnal and seasonal thermoclines. (d) Three-layer approximation of the continuous stratification, where the layer separation occurs at the upper and lower surfaces of the metalimnion. (e) Continuous stratification throughout the water column with constant buoyancy frequency. (f) Continuous stratification where the hypolimnion is characterized by a constant buoyancy frequency.

difference between water surface and adjacent air column.

The momentum transfer associated with steady winds will push the surface water to the leeward shore, causing a displacement of the free surface due to the presence of the solid boundary (Figure 2a); for long and shallow lakes this may be as large as several meters (e.g., ~2 m in Lake Erie) (see **Currents in the Upper Mixed Layer and in Unstratified Water Bodies**).

This displacement is called wind set-up. If the wind stress is applied for sufficient time (one quarter of the fundamental seiche period as defined below), a steady-state tilt of the free surface will occur where there is a balance between the applied wind force ($\tau \times$ surface area) and the hydrostatic pressure force due to the desire of the free surface to return to gravitational equilibrium. Balancing these forces at steady state, given the equation for the slope of the free surface

$$\frac{\partial \eta_s}{\partial x} = \frac{u_*^2}{gH}$$

where $u_* = \sqrt{\tau/\rho_o}$ is the surface wind shear velocity, $\eta_s(x,t)$ is the interfacial (surface) displacement from the equilibrium position, and x is the longitudinal coordinate. The equation for the free-surface slope may be integrated to give the maximum interfacial displacement, as measured along the vertical boundary

$$\eta_s(t = 0, x = 0, L) = \pm \frac{u_*^2}{gH}\frac{L}{2}$$

Wind Set-Up of the Internal Stratification

In a manner analogous to the set-up at the free surface, wind induced displacements can also occur along the thermocline. Consider a simple two-layered lake. Water piled-up at the leeward shore by windward drift simultaneously pushes down the thermocline while pushing up the free surface (Figure 2(b), Figure 3). The free surface remains nearly horizontal owing to a return flow that develops in the hypolomnion, leading to vertical velocity shear through the metalimnion. A corresponding upwelling occurs at the windward shore (Figure 3). The steady-state slope of the free surface is given by a balance between the baroclinic gravitational pressure force from the tilted thermocline and the force due to the wind-stress acting through the epilimnion

$$\frac{\partial \eta_i}{\partial x} = \frac{u_*^2}{g' h_1}$$

where $g' = g(\rho_2 - \rho_1)/\rho_2$ is the reduced gravity across the interface (thermocline) (see **Currents in Stratified Water Bodies 1: Density-Driven Flows**). The equation for the thermocline slope may be obtained through integration over the basin length

$$\eta_i(t = 0, x = 0, L) = \pm \frac{u_*^2}{g' h_1}\frac{L}{2}$$

The effect of buoyancy can be seen by decreasing the density difference between the two layers resulting in a decrease in g' and corresponding increase in η_i.

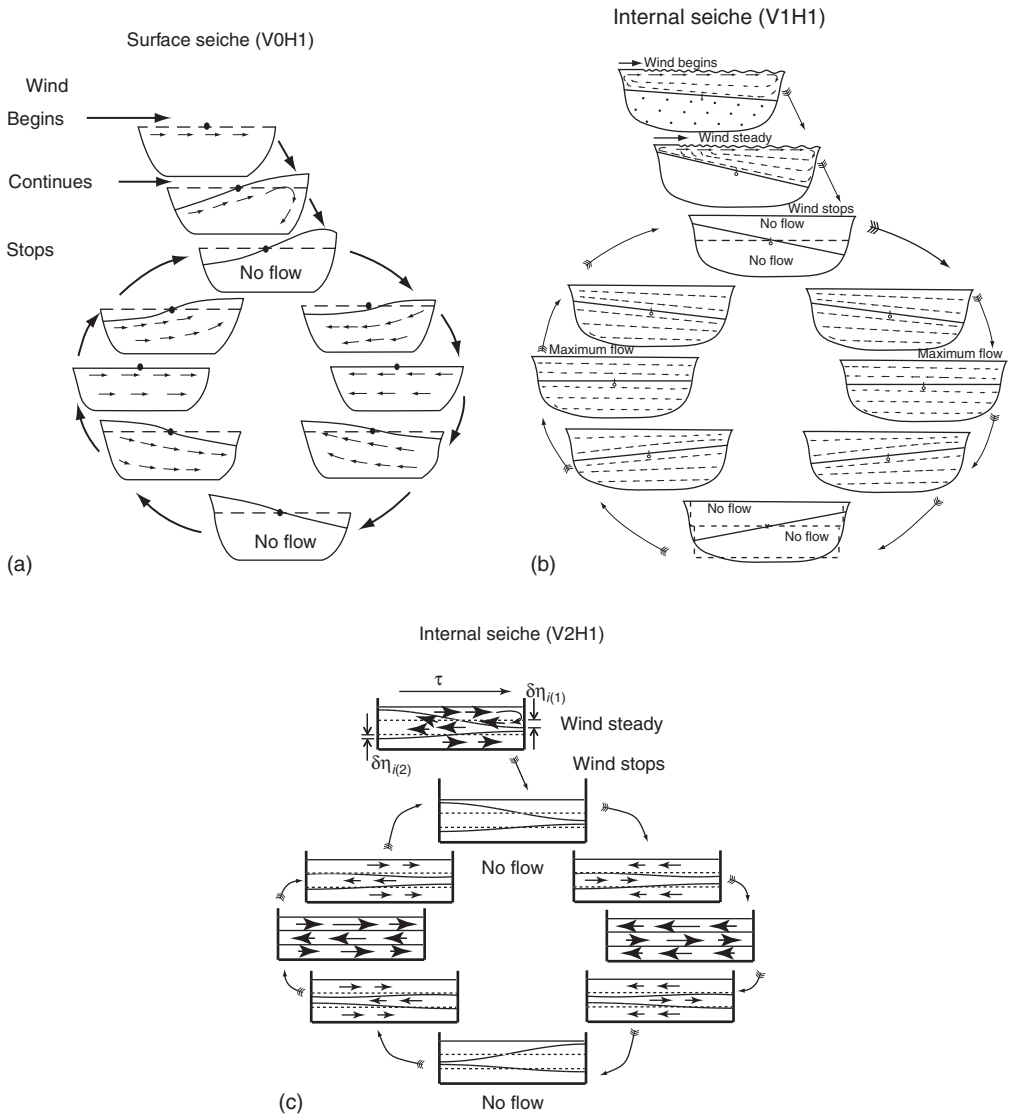

Figure 2 Movement caused by steady moderate wind stress on a hypothetical layered lake and subsequent internal seiche motion neglecting damping. (a) Horizontal mode one surface seiche in a homogeneous one-layered system, (b) horizontal mode one vertical mode on internal seiche in a two-layered system, both adapted from Mortimer CH (1952) Water movements in lakes during summer stratification: Evidence from the distribution of temperature in Windermere. *Proceedings of the Royal Society of London Series B*. 236: 355–404 and (c) horizontal mode one vertical mode two internal seiche in a three-layered system. Arrows denote distribution and magnitude of water particle velocities. At $t = 0$, $(1/2)T_1$, T_1, $(3/2)T_1$, etc. the wave energy is purely in the potential form, isotherms are at their maximum tilt and there is no seiche induced flow, while at $t = (1/4)T_1$, $(3/4)T_1$, $(5/4)T_1$, etc. the energy is purely kinetic, giving rise to strong horizontal currents within the lake-basin and horizontal isotherms.

A simple comparison $\eta_s/\eta_i \sim (\Delta\rho/\rho_o)(b_1/H)$ shows that for weakly stratified deep systems, internal displacements (~1–100 m) may be more than an order of magnitude greater than their surface counterparts (~0.01–1 m); for example in Lake Baikal $\eta_s/\eta_i \sim 0.11\text{m}/75\text{ m} \sim 10^{-3}$.

The available potential energy (APE) embodied in the tilted interface is readily calculated for a two-layer system by integrating the interfacial displacement over the basin length

$$\text{APE} = g\frac{\rho_2 - \rho_1}{2}\int_0^L \eta_i^2(x,t)dx$$

which may be integrated for the initial condition of a uniformly tilted thermocline

$$\text{APE} = \frac{1}{6}gL(\rho_2 - \rho_1)\eta_i^2$$

After the thermocline tilt has reached steady state, work done by continued winds is either dissipated

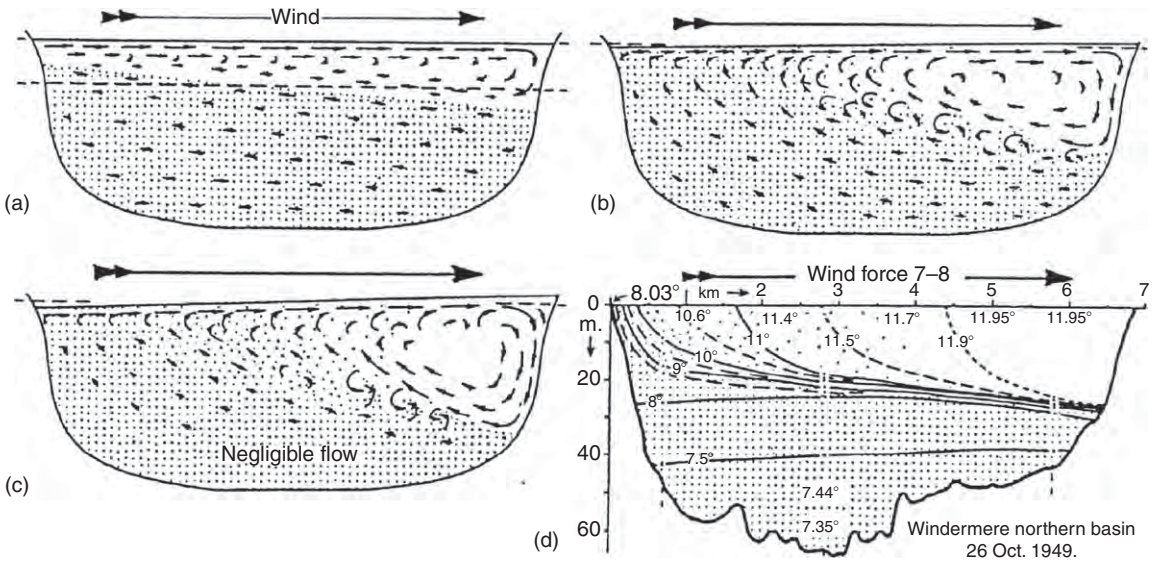

Figure 3 Schematic showing the response of a stratified lake to a surface wind stress. (a–c) show the stages of development of a steady state thermocline tilt. The hypolomnion is shaded and the arrows show the relative speed and direction of the flow. (d) Isotherm distribution and temperatures in Lake Windermere, northern basin, after a steady wind for 12 h. Reprinted from Mortimer CH (1954) Models of the flow-pattern in lakes. *Weather* 9: 177–184.

internally as heat or acts to mix the water column by further deepening the surface layer. Surface layer deepening has been characterized into four distinct regimes based on the strength of the stratification and winds (Figure 4 and see **The Surface Mixed Layer in Lakes and Reservoirs**). For strong stratification and weak winds (Regime A) the thermocline set-up is small, internal seiches persist for long times, mixing is weak and the thermocline remains sharp. If the stratification is weaker or the winds stronger (Regimes B and C), seiche amplitudes increase and become a predominant feature, shear instabilities (e.g., Kelvin–Helmholtz billows) form leading to entrainment of the metalimnion into the epilimnion, enhanced mixing and causing rapid damping of the internal seiches. For weak stratification and strong winds (Regime D), shear instabilities are strong; the thermocline becomes diffuse with a steep slope and rapidly deepens toward the lake bed. This creates a sharp downwind interface and a broad upwelling at the upwind shore. The upwelled fluid creates a longitudinal temperature gradient, which subsequently mixes the lake horizontally. The colder upwelled water is nutrient rich and as it mixes rapid fluctuations in temperature and biogeochemistry result. In deeper lakes, stratification can be strong during summer and upwelling of metalimnetic (partial upwelling) or hypolimnetic (full upwelling) water is unlikely. In these lakes upwelling is favored just after spring turnover or prior to fall turnover when the thermal stratification is weak or near the surface.

Wedderburn and Lake Numbers

The degree of tilt of the base of the surface layer resulting from an applied wind stress may be quantified using the dimensionless Wedderburn number W, which as the ratio of the wind disturbance force to the gravitational baroclinic restoring force is given by

$$W \sim \frac{g' h_1^2}{L u_*^2}$$

Here, g' is evaluated across the base of the surface layer. The cases of $W \gg 1$, $W \sim 1$ and $W \ll 1$ correspond to Regimes A, B/C, and D, respectively.

For idealized laboratory studies and back-of-the-envelope calculations, substitution of η_i into the equation for W leads to a leads to two-layer form

$$W \sim \frac{h_1}{\delta\eta_i}$$

where $\delta\eta_i$ is the steady wind induced vertical displacement of the seasonal/diurnal thermocline measured at the boundary. Due to the order of magnitude scaling, the factor of 2 has been dropped as is commonly found in the scientific literature. Moreover, the somewhat counterintuitive nature of $W \to \infty$ as $\delta\eta_i \to 0$, leads to frequent use of the inverse form of the Wedderburn number ($W^{-1} \sim \delta\eta_i / h_1$).

For lakes which are not well approximated using a two-layer stratification, W has been generalized into the Lake Number, L_N (see **Density Stratification and Stability**). This accounts for the depth

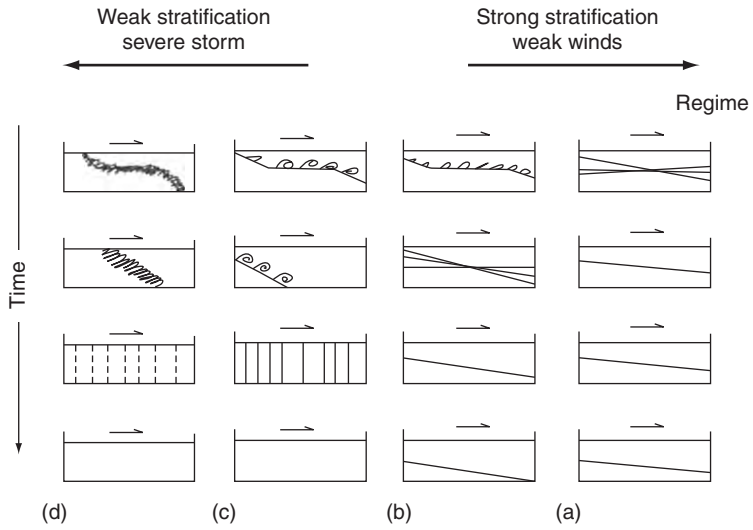

Figure 4 Schematic showing the mixed layer deepening response of a lake to wind stress. (a) Regime A: internal waves; (b) Regime B: internal waves and slight billowing; (c) Regime C: strong billowing and partial upwelling; (d) Regime D: intense billowing and full upwelling. Adapted From Fischer HB, List EJ, Koh RCY, Imberger J, and Brooks NH (1979). *Mixing in Inland and Coastal Waters*. San Diego, CA: Academic Press. After Spigel RH, and Imberger J (1980) The classification of mixed layer dynamics in lakes of small to medium size. *Journal of Physical Oceanography* 10: 1104–1121.

dependence of stratification and horizontal area. For a constant wind stress over a lake with an arbitrary basin shape and stratification

$$L_N = \frac{S_t(H - h_2)}{u_*^2 A_o^{3/2}(H - h_v)}$$

Here A_o is the surface area of the lake and h_v is the height from the lake-bed to the centre of volume of the lake. The stability of the lake

$$S_t = \frac{g}{\rho_o}\int_0^H (z - h_v)A(z)\rho(z)dz$$

incorporates the variable stratification $\rho(z)$ and irregular bathymetric area $A(z)$. For large Lake numbers, the stratification will be severe and dominate the forces introduced by the wind stress. The isotherms will be horizontal, with little or no seiching and associated turbulent mixing in the benthic boundary layer and interior. Changes in S_t with latitude and season cause L_N to vary spatially and temporally around the globe (see **Mixing Dynamics in Lakes Across Climatic Zones**). Under comparable wind conditions L_N is maximal in the mid-latitudes during summer.

Basin-Scale Standing Wave Motions (Seiches)

Interfacial Waves in a Layered Stratification

Horizontal modes When steady winds cease and the surface stress condition is relaxed, the gravitational restoring force associated with the tilted interface (water surface or thermocline) becomes unbalanced. The available potential energy embodied in the tilt is released under the action of gravity and converted to kinetic energy as the interface oscillates in the form of a sinusoidal standing waves or seiche. Antinodes are found at the basin end walls and nodal points in the basin interior (Figures 2 and 5). Seiches are commonly called linear waves because the evolving wave-field is well described in space and time by the linear wave equation

$$\frac{\partial^2\eta}{\partial t^2} = c_o^2\frac{\partial^2\eta}{\partial x^2}$$

where $\eta(x,t)$ is the interfacial displacement and c_o the linear shallow water phase speed (speed at which the crests/troughs propagate). This equation is equally applicable to interfacial waves travelling on the free-surface or thermocline by applying the appropriate form of $c_o = \sqrt{gH}$ or $c_o = \sqrt{g'h_1h_2/H}$, for the cases of surface and internal seiches, respectively. Due to the reduced effect of gravity across the thermocline relative to the free surface ($g' \ll g$), surface waves travel at ~50 times the speed of internal waves.

The familiar standing wave patterns associated with seiches forms as symmetric progressive waves of equal amplitude and wavelength, but opposite sign, propagate from the upwelled and downwelled fluid volumes at the opposite ends of the basin (Figure 2). These waves are most commonly represented with cosine functions (Figure 5), which have central node(s) and antinodes at the basin walls. Summing cosine

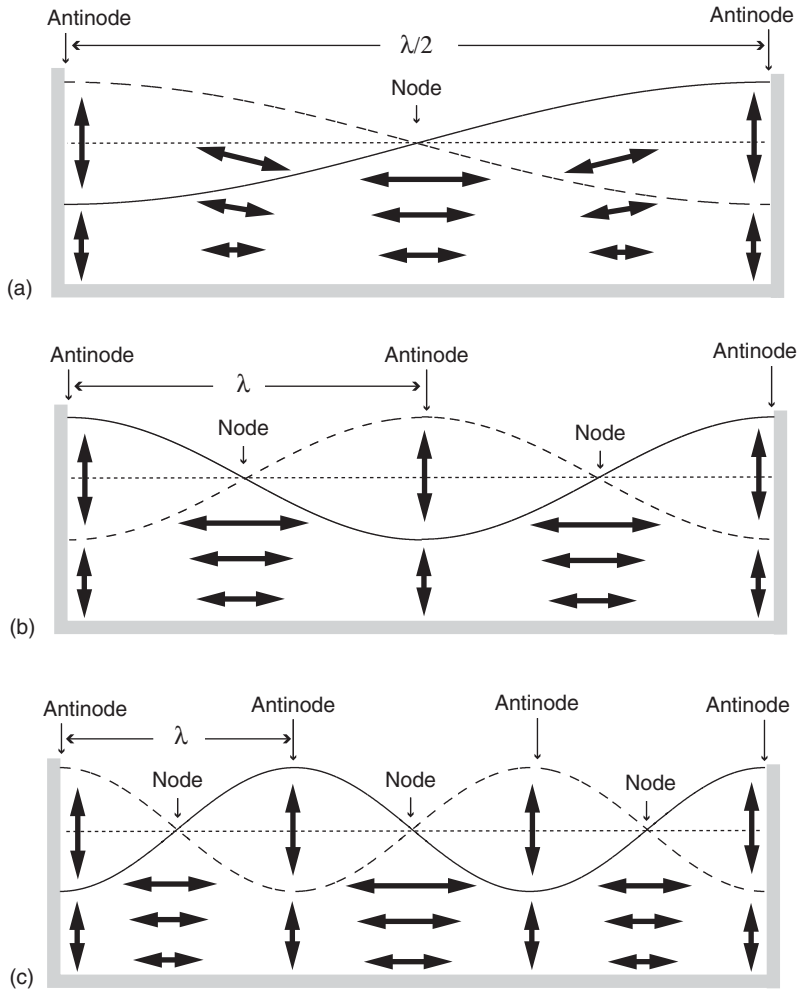

Figure 5 Schematic diagram showing the first three horizontal interfacial seiche modes: horizontal mode one (n = 1), mode two (n = 2), and mode three (n = 3). Arrows denote direction of water particle velocities. Solid and dashed lines denote the interfacial displacement at one-half period intervals. Upper layer velocities for the baroclinic case are not shown and can be inferred from symmetry.

equations for waves propagating in opposite directions, gives the equation for the horizontal mode one (H1) standing wave pattern (Figure 5(a))

$$\eta(x,t) = a\cos(kx+\omega t) + a\cos(kx-\omega t) = 2a\cos kx\cos\omega t$$

The component wave amplitude $a = \delta\eta_i/2$ or $\delta\eta_s/2$ depending on the interface under consideration, the angular frequency $\omega = c_o k$, where $k = 2\pi/\lambda$ is the wavenumber and λ the wavelength and $T = 2\pi/\omega$ the wave period. For an enclosed basin, there is one half wavelength of an H1 seiche in a lake, giving $\lambda = 2L$ and a period of

$$T_n = \frac{2L}{nc_o}$$

where $n = 1$ for a H1 seiche is the number of nodal points or half wavelengths in the horizontal direction.

The layer-averaged horizontal velocities associated with the H1 seiche are maximum the centre of the basin and are given by

$$U_1 = g'\frac{b_2}{H}\frac{\delta\eta_i}{L/2}t$$

$$U_2 = g'\frac{b_1}{H}\frac{\delta\eta_i}{L/2}t$$

These velocities are zero at the vertical boundaries, where the motion is purely vertical (Figure 5). Similarly for the surface seiche, the mid-lake depth-averaged velocity is

$$U = g\frac{\delta\eta_s}{L/2}t$$

The oscillatory seiche currents are low-period and quasi-steady. Observations from a variety of lakes and reservoirs show the surface and internal seiche

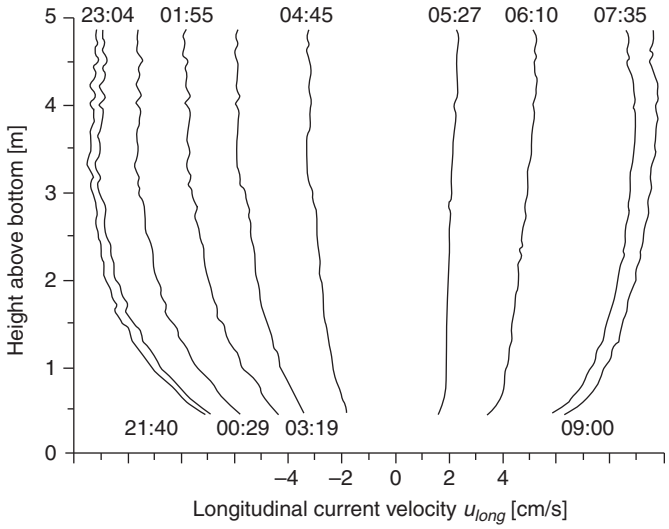

Figure 6 Near-bed velocity profiles in a small lake showing the oscillatory nature and no-slip boundary associated with seiche currents. Observations are over one-half of the seiche period taken at times as indicated. The profiles are offset and are all plotted with the given velocity scale. From Lorke A, Umlauf L, Jonas T, and Wüest A (2002) Dynamics of turbulence in low-speed oscillating bottom boundary layers of stratified basins. *Environmental Fluid Mechanics* 2: 291–313.

currents to have a typical range of 0.02–0.20 m s^{-1}, with a maximum ~0.2 m s^{-1} during storms and to approach zero at the no-slip sediment boundary where the flow is impeded by friction (Figure 6).

Higher horizontal mode seiches ($n > 1$) are also observed in lakes. These are described by a more general solution of the linear wave equation, where the initial condition is that of a uniformly tilted interface, made up of the superposition of all higher horizontal modes. The general solution is

$$\eta(x,t) = \sum_{n=1}^{\infty} \left(\frac{-8\delta\eta}{n^2\pi^2}\right) \cos\left(\frac{n\pi}{L}x\right) \cos\left(\frac{c_o n\pi}{L}t\right) \quad n = 1, 3, 5, \ldots$$

$n = 1$ for the horizontal mode-one (H1) seiche, $n = 2$ for the horizontal mode-two (H2) seiche, $n = 3$ for the horizontal mode-three (H3) seiche (Figure 5). An infinite number of modes are possible, each with decreasing amplitude and energy as the modal number increases. The fundamental solution is composed only of odd modes (i.e., $\eta(x,t) = 0$ when n is even) as is intuitively expected because only odd odes have a nodal point at the mid-basin location where there is zero displacement associated with an initial uniform initial tilt (Figures 2 and 3). By calculating the APE associated with each mode, it can be shown that that more than 98% of the wave energy is contained in the H1 mode, but the energy distribution between modes may be significantly affected by resonant forcing and basin shape.

Examples of surface and internal seiche periods for various horizontal modes are given in Table 1. Energy will pass between potential and kinetic forms as the wave periodically oscillates with time (Figure 2). At $t = 0$, $(1/2)T_1$, T_1, $(3/2)T_1$, etc. the wave energy is purely in the potential form, while at $t = (1/4)T_1$, $(3/4)T_1$, $(5/4)T_1$, etc. the energy is purely kinetic, giving rise to horizontal currents within the lake-basin (Figure 6). For a non dissipative system, the modal energy distributions represent the sum of kinetic and potential energy and are independent of time. Dissipative processes will lead to a decrease in wave amplitude, but not period, with time (Table 1); unless there is sufficient mixing across the thermocline to cause a change in the stratification and hence c_o. For surface seiches the decay in amplitude with each successive period can range from 3% (Lake Geneva) to 32% (Lake Erie).

Vertical modes When the vertical density structure may be approximated with three or more fluid layers (Figure 1c,d), in addition to vertical mode-one, horizontal mode-one (V1H1) seiches (Figure 2b), higher vertical mode seiches are supported; for example V2H1, etc. (Figure 2c). For a three-layer system c_o becomes

$$c_o = \frac{1}{2H}\left(\gamma - \sqrt{\gamma^2 - 4\alpha H}\right)$$

where

$$\gamma = (1 - \rho_1/\rho_2)h_1h_2 + (1 - \rho_1/\rho_3)h_1h_3 + (1 - \rho_2/\rho_3)h_2h_3$$

and

$$\alpha = h_1h_2h_3(1 - \rho_1/\rho_2)(1 - \rho_2/\rho_3).$$

Substitution into the equation for the wave period $T_n = 2L/nc_o$ gives the period of a vertical mode-two

Table 1 Observed surface and internal seiche periods from a variety of lakes and the associated amplitude decay

Lake and location	T_1 (*h*)	T_2 (*h*)	T_3 (*h*)	T_4 (*h*)	T_5 (*h*)	*Fractional decrease in amplitude with each successive period*
Surface seiches						
Tanganyika (Africa)[1]	0.075	0.038	0.028			
Loch Earn (Scotland)[1]	0.24	0.14	0.10	0.07	0.06	
Yamanaka (Japan)[1,2]	0.26	0.18	0.09			0.099
Garda (Italy)[1,2]	0.72	0.48	0.37	0.25	0.20	0.045
Geneva (Switzerland–France)[1,2]	1.2	0.59				0.030
Vättern (Sweden)[1,2]	3.0	1.6	1.3	0.97	0.80	0.113
Baikal (Russia)[1]	4.6					
Michigan (Canada–USA)[1]	9.1	5.2	3.7	3.1	2.5	
Erie (Canada–USA)[1,2]	14.3	9.0	5.9	4.2		0.322
Internal seiches						
Baldegg (Switzerland)[3]	9.3	4.6	3.1	2.1		
Lugano (Switzerland–Italy)[4]	24	12	8.0	6.2		
Windermere (England)[3]	24	13	9			
Zurich (Switzerland)[5]	45	24	17			
Loch Ness (Scotland)[3]	57	27	18	14	11	
Geneva (Switzerland–France)[3]	74	46	30	22	18	

[1]Wilson W (1972) Seiches. In Chow VT (ed.) *Advances in Hydroscience* 8: 1–94.
[2]Wüest AJ and Farmer DM (2003) Seiches. In *McGraw-Hill Encyclopedia of Science and Technology*, 9th Edition. New York: McGraw-Hill.
[3]Lemmin U and Mortimer CH (1986) Tests of an extension to internal seiches of Defant's procedure for determination of surface seiche characteristics in real lakes. *Limnology and Oceanography* 31: 1207–1231.
[4]Hutter K, Salvadè G, and Schwab DJ (1983) On internal wave dynamics in the northern basin of the Lake of Lugano. *Geophysical and Astrophysical Fluid Dynamics* 27: 299–336.
[5]Horn W, Mortimer CH and Schwab DJ (1986) Wind-induced internal seiches in Lake Zurich observed and modeled. *Limnology and Oceanography* 31: 1232–1254.

wave, where the horizontal modal structure is defined by n.

Vertical mode-two seiches can be generated when there is an asymmetry in the tilting of upper and lower interfaces of the stratifying layers (the diurnal and seasonal thermoclines or the upper and lower boundaries of the metalimnion). Laboratory and limited field data shows that such asymmetries are introduced from the compression and expansion of the metalimnion that occurs along the downwind and upwind shores, respectively, under upwelling conditions (e.g., **Figure 3(d)**). The strength of the vertical mode two response has been hypothesized to depend upon the relative values of the Wedderburn and Lake Numbers. A V2 response occurs for small W and large L_N (strong tilting of the upper interface, large shear across the base of the surface layer and a relatively undisturbed lower interface); whereas a V1 response occurs for small W and large L_N (comparable tilts of both interfaces and a strong velocity in the hypolimnion).

Higher vertical mode basin-scale internal waves have been observed in several lakes, generally after a sudden wind pulse has excited an initial V1H1 response, which then evolves into a V2 seiche (e.g., Wood Lake, Upper Mystic Lake, Lake Constance). Resonance with the wind forcing (e.g., Lake Alpnach), sloping basin topography and unequal density differences between stratifying layers can cause this preferential excitation of higher vertical modes.

Internal Modes in a Continuous Stratification

The two-layer assumption for the stratification in lakes is inappropriate for the many shallow lakes ($H < \sim 15$ m; e.g., Frains Lake) and in the hypolomnion of lakes that are very deep (e.g., Lake Baikal) or where the stratification has a significant chemical (saline) component (e.g., Mono Lake). These systems are better modeled using a continuous stratification where the tilting of the isopycnals due to wind set-up is captured by L_N. Upon relaxation of a wind stress, a continuous stratification will support a spectrum of vertical basin-scale modes. The frequency associated with each mode is given by

$$\omega = \frac{N}{\left(1 + \frac{n^2}{m^2}\frac{L^2}{H^2}\right)^{1/2}}$$

which is dependent upon the basin geometry and may be used to calculate the wave period $T = 2\pi/\omega$. The structure of each vertical mode m is described by the wavefunction ψ_m, which is obtained from the linear long-wave equation with constant N

$$\psi_m(z) = \sin\left(\frac{m\pi}{H}z\right) \text{ and } c_o = \pm\frac{NH}{m\pi}\, m = 1, 2, 3, \ldots.$$

and is a measure of the wave-induced vertical displacement of the internal strata at a particular depth. For example, the V1 wave has a maximum internal displacement at mid-depth, whereas the V2 wave has a positive displacement at $1/4H$ and a negative displacement at $3/4H$ (Figure 7a); showing the characteristic opening of the strata.

The wavefunction contains no knowledge of the actual wave amplitude and consequently is often normalized $-1 \leq \psi_m \leq 1$. The utility of ψ_m is that it may be numerically calculated from the Taylor–Goldstein equation for an arbitrary $N(z)$ profile, thus determining the wave modes that are supported by a particular water column stratification. The basin-scale vertical modal structure, either a single mode or combination of modes, may be calculated when the wave amplitude is known $\eta(z,t) \approx \psi_m(z)a(t)$. The vertical modal structure can then be projected in space and time throughout the basin by assuming a wave profile $\eta(x,z,t) \approx \psi_m(z)\eta(x,t)$; this is typically a cosine for seiches or sech^2 function for solitary waves (described later).

The horizontal velocity profile induced by the wave motion scales with the gradient of the wavefunction $c_o d\psi_m/dz$ (Figure 7(b)). Analytical expressions for the velocity field can be found in stratified flow texts. The continuous velocity profiles in Figure 7 are consistent with the depth averaged currents presented in Figure 2. In both models, although technically incorrect (Figure 6), a free-slip bottom boundary has been assumed. Accordingly the velocities from these models are not representative of flow near the bottom boundary.

Degeneration of Basin-Scale Internal Waves in Lakes

Understanding the factors leading to wave degeneration has been a major goal of limnologists. This is because internal waves ultimately lose their energy (degenerate) to dissipation (viscous frictional heating of the fluid at mm scales) and diapycnal mixing (mixing of fluid perpendicular to isopycnals or surfaces of constant density) in regions where the flow is turbulent. In turn, mixing drives biogeochemical fluxes. Turbulence is produced directly from the seiche induced currents through fluid straining in the lake interior and TBBL, and from processes that are uncoupled from seiche generation, such as surface wave breaking and inflows, which also act to disrupt the seiche motion. As a general rule, for deep lakes, the period of internal seiche decay is about 1 day per 40 m of water-column

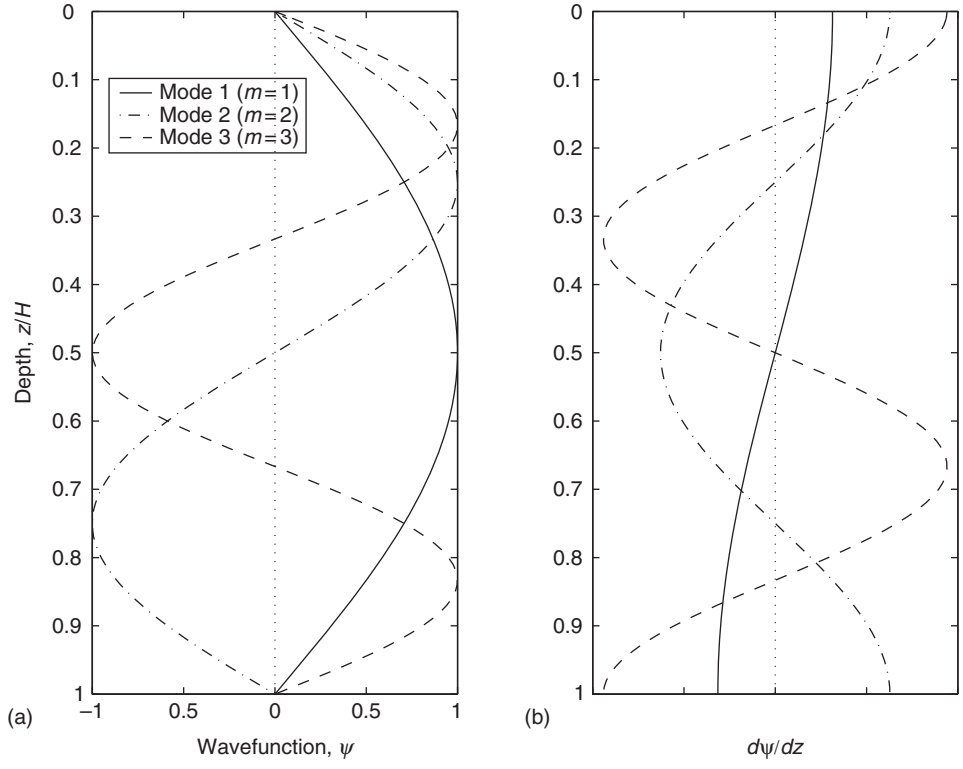

Figure 7 (a) Wavefunction profiles for vertical modes one ($m = 1$), two ($m = 2$), and three ($m = 3$) supported by a constant N stratification. (b) Characteristic velocity profiles $c_o d\psi/dz$ for wavefunctions shown in panel (a).

depth. For very deep lakes, e.g., Lake Baikal where $H = 1637$ m, this equates to a decay period of more than one month.

Field observations show the degeneration of basin scale internal waves to occur primarily as a result of turbulence production in the TBBL rather than the interior; observations of dissipation and mixing are more than ten times greater in the TBBL than the interior (see **The Benthic Boundary Layer (in Rivers, Lakes and Reservoirs)**). The degeneration can occur through four possible mechanisms: (1) viscous damping of seiche currents in the TBBL, (2) the formation of shear instabilities in the interior, (3) the production of nonlinear internal waves that will break on sloping topography; and (4) the formation of internal hydraulic jumps. By calculating the timescales over which each mechanism will occur, regimes have been delineated in which a particular mechanism will dominate (Figure 8). The regimes are defined according to the inverse Wedderburn number $W^{-1} = \delta\eta_i/h_1$ and the depth of the seasonal thermocline (h_1/H). Although strictly applicable to long narrow lakes that match the rectangular system used in the analysis, the regime diagram has been shown to suitably predict field observations from a variety of lakes (Table 2). The degeneration regimes are described below.

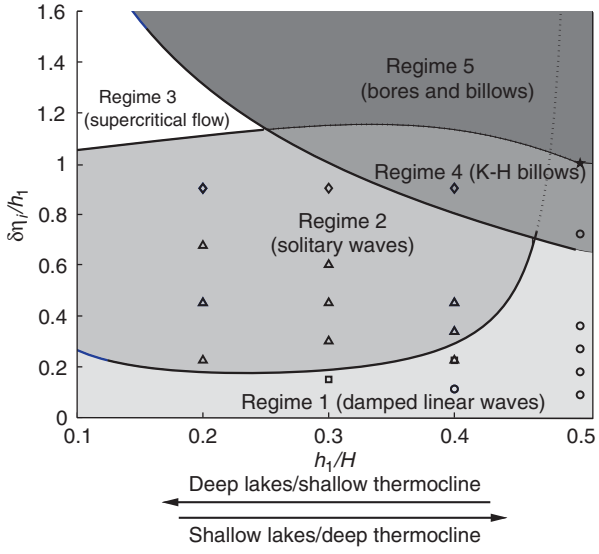

Figure 8 Analytical regime diagram showing the degeneration mechanisms of seiches in long rectangular lakes. The regimes are characterized in terms of the normalized initial forcing scale $W^{-1} = \delta\eta_i/h_1$ and the depth of the seasonal thermocline (h_1/H). Laboratory observations are also plotted (*, Kelvin–Helmholtz (K-H) billows and bore; ◊, broken undular bore; Δ, solitary waves; □, steepening; ○, damped linear waves). From Horn DA, Imberger J, and Ivey GN (2001) The degeneration of large-scale interfacial gravity waves in lakes. *Journal of Fluid Mechanics* 434: 181–207.

Regime 1: Damped Linear Waves

Under relatively calm conditions ($W^{-1} < \sim 0.2$) weak seiches develop, which are damped by viscosity in the TBBL. Seiche amplitudes and currents are not sufficient for solitary wave production, shear instability and/or supercritical flow. This regime corresponds to regime A in Figure 4 (see **The Surface Mixed Layer in Lakes and Reservoirs**). The time scale associated with viscous damping of a basin-scale seiche T_D is estimated from the ratio of the seiche energy to the rate of energy dissipation in the benthic boundary layer ϵ_{TBBL}:

$$T_D \sim \frac{\text{Seiche energy}}{\epsilon_{TBBL}} \times \frac{\text{Lake volume}}{\text{TBBL volume}} \sim 1 \text{ to } 10 \text{ d} (\text{for moderately sized lakes})$$

The energy dissipation in the lake interior $\epsilon_{Interior}$ is neglected because observational studies show that $\epsilon_{TBBL} > 10\epsilon_{Interior}$ (see **The Surface Mixed Layer in Lakes and Reservoirs**). More complex models for viscous seiche decay may be found in references below.

Regime 4: Kelvin–Helmholtz Billows

Kelvin–Helmholtz instabilities can form due to a number of mechanisms. Under strong forcing conditions and as the thermocline approaches mid-depth (> ~0.8 and > ~0.3), the seiche-induced currents will be sufficiently strong to overcome the stabilizing effects of stratification. Shear instabilities will occur before solitary waves can be produced and/or the seiche is damped by viscosity. Shear from other processes, such as the surface wind stress, can augment that from seiche induced currents and induce instabilities under weaker forcing conditions.

Shear instabilities manifest themselves as high-frequency internal waves that are common features through the metalimnion of lakes and oceans. The waves are the early stages of growth of the instabilities and have sinusoidal profiles, frequencies $\sim 10^{-2}$ Hz, wavelengths ~10–50 m and amplitudes ~1–2 m. Depending on the particulars of the stratification and velocity shear profiles, the shear instabilities may be classified according to their profile (e.g., Kelvin– Helmholtz billows, Holmboe waves or combinations thereof). Instabilities grow exponentially from small random perturbations in the flow, leading to rapid degeneration as patches of localized turbulent mixing or billowing (see **Small-scale Turbulence and Mixing: Energy Fluxes in Stratified Lakes**). This process is shown schematically in Figure 9.

In a continuously stratified flow, the stability behavior is governed by the Taylor–Goldstein

Table 2 Comparison between predicted regime and observations in several lakes

Lake	*Dates*	*Observations*	*W* (W^{-1})	*Regime*	*Source*
Loch Ness	Oct. 2–3, 1971	'Pronounced front or surge'	3 (0.3)	2	1
Lake of Zurich	Sept. 11–14, 1978	'Steep fronted solitary wave'	3 (0.3)	2	2
Windermere	Aug. 14–20, 1951	'Damped harmonic oscillations'	5 (0.2)	1–2	3
	Sept. 13–17, 1951	'Oscillatory waves' with some steepening	3 (0.3)	1–2	
Babine Lake	July 5–10, 1973	'Surges'	2 (0.5)	2	4
	Aug. 12–15, 1973	'Steep shock front'	3 (0.3)	2	
	Oct. 2–7, 1973	'Surges' and 'solitary waves'	2 (0.5)	2	
Seneca Lake	Oct. 14–21, 1968	'Surges' consisting of trains of 'solitons'	2 (0.5)	2	5
Kootenay Lake	July 13–Aug. 17, 1976	'Surges' consisting of waves resembling 'solitons'	2 (0.5)	2	6
Balderggersee	Nov. 1–15, 1978	'Asymetrical waves'	9 (0.1)	2	7
	Nov. 16–22, 1978	'Steepened wave front. . .described as an internal surge'	2 (0.5)	2	
Lake Biwa	Sept. 4–13, 1993	'Undular bores and solitary waves'	1 (1)	2	8

Most observations fall in regime 2 ($W^{-1} > \sim 0.3$) and the internal seiche will degenerate into nonlinear internal waves. For Windermere, the baroclinic tilting is weaker ($W^{-1} < \sim 0.3$) and the predominant response is a damped seiche. After Horn DA, Imberger J, and Ivey GN (2001) The degeneration of large-scale interfacial gravity waves in lakes. *Journal of Fluid Mechanics* 434: 181–207.

Sources

1. Thorpe SA, Hall A, and Crofts I (1972) The internal surge in Loch Ness. *Nature* 237: 96–98.
2. Mortimer CH and Horn W (1982) Internal wave dynamics and their implications for plankton biology in the Lake of Zurich. *Vierteljahresschr. Naturforsch. Ges. Zurich* 127(4): 299–318.
3. Heaps NS and Ramsbottom AE (1966) Wind effects on the water in a narrow two-layered lake. *Philosophical Transactions of the Royal Society of London A* 259: 391–430.
4. Farmer DM (1978) Observations of long nonlinear internal waves in a lake. *Journal of Physical Oceanography* 8: 63–73.
5. Hunkins K and Fliegel M (1973) Internal undular surges in Seneca Lake: A natural occurrence of solitons. *Journal of Geophysical Research* 78: 539–548.
6. Wiegand RC and Carmack E (1986) The climatology of internal waves in a deep temperate lake. *Journal of Geophysical Research* 91: 3951–3958.
7. Lemmin U (1987) The structure and dynamics of internal waves in Baldeggersee. *Limnology and Oceanography* 32: 43–61.
8. Saggio A and Imberger J (1998) Internal wave weather in a stratified lake. *Limnology and Oceanography* 43: 1780–1795.

equation, from which it can be shown that a gradient Richardson number

$$Ri_g = \frac{N(z)^2}{(du/dz)^2} < \frac{1}{4}$$

is a necessary but not sufficient condition for instability (Miles-Howard criterion). Billowing occurs along thin layers in the flow (~10 cm thick) where Ri_g is low and there are interfaces with sharp density gradients. Through billowing, the interfaces become more diffuse and are replaced by shear layers of thickness $\delta \sim 0.3(\Delta U)^2/g'$, where ΔU is the velocity jump over the interface. As a result of billowing, the flow becomes stable unless ΔU increases (e.g., due to increasing wind stress) or δ decreases (e.g., due to mixed layer deepening). A spectrum of growing instabilities are theoretically possible, but the most unstable mode wave will have a wavelength $\lambda = 2\pi/k \sim 7\delta$.

Application of the Taylor–Goldstein equation to field observations shows that the frequency of the most unstable mode is just below the maximum buoyancy frequency through the metalimnion. This is because a fluid parcel displaced vertically from its equilibrium density position, as occurs during the growth of an instability, will be subjected to buoyancy forces arising from the sudden density anomaly with respect to its surroundings. The fluid parcel will oscillate as a wave at frequency N until the motion is frictionally damped by viscosity or evolves into a billow and collapses into turbulence. Fluid parcels will not naturally oscillate at frequencies greater than N, and so waves will not propagate at these frequencies; N is thus the limiting high-frequency cut-off for internal wave motions.

Internal seiches generate substantial vertical shear due to the baroclinic flow reversals across layer interfaces (Figures 2–5). The magnitude of this shear is periodic and has a maximum value when the interfaces are horizontal (e.g., $T_1/4$) and all wave energy is in the kinetic form. A bulk Ri may be applied over the interfaces separating discrete layers

$$Ri = \frac{g'\delta}{(\Delta U)^2} < \frac{1}{4}$$

to predict the formation of instabilities. If the background flow is time-variable, either the condition $Ri = 1/4$ must be maintained for longer than the growth and billowing period of the instability $T_b \sim 20(\Delta U)/g'$ or Ri must be $<<1/4$. Values of T_b in lakes are of the order of minutes or less.

Shear instabilities can occur at the nodal locations in lakes, where the vertical shear is greatest, at the base of the surface layer under strong wind

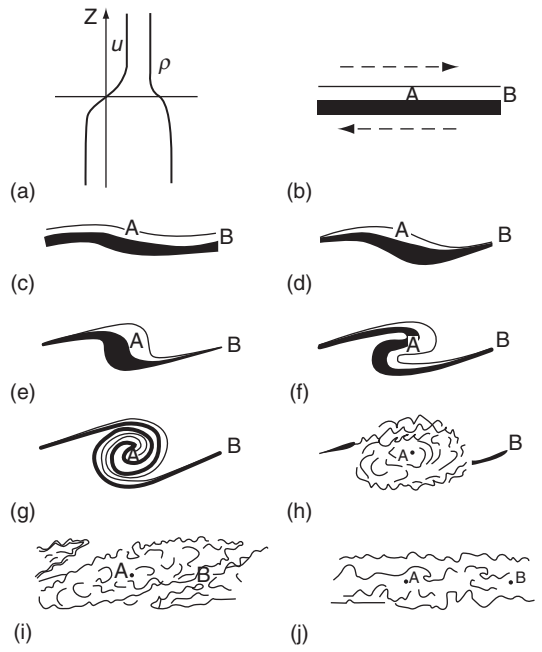

Figure 9 Schematic showing the growth and turbulent degeneration of a Kelvin–Helmholtz shear instability leading to diapycnal mixing of the stratified fluid. The condition is shown as velocity (u) and density (ρ) profiles in (a) and as isopycnal surfaces in (b), where the arrows denote the flow direction. In (b–j), A and B are fixed points in the flow and the lines represent surfaces of constant density (isopycnals). Adapted from Mortimer CH (1974). Lake hydrodynamics. *Mitteilungen Int Ver Limnol* 20: 124–197, after Thorpe SA (1987) Transitional phenomena and the development of turbulence in stratified fluids: A review. *Journal of Geophysical Research* 92: 5231–5248.

conditions, on the upper and lower surfaces of thermocline jets that result from vertical mode-two compression of the metalimnion, near river influents and reservoir withdrawal layers, and in regions where there is flow over rough topography.

Regime 3: Supercritical Flow

Internal hydraulic jumps occur in stratified flows at the transition from supercritical ($Fr_1^2 + Fr_2^2 > 1$) to subcritical ($Fr_1^2 + Fr_2^2 < 1$) flow conditions, where the upper and lower layer Froude numbers are defined as $Fr_1^2 = U_1^2/g'h_1$ and $Fr_2^2 = U_2^2/g'h_2$. Although they are more commonly observed in the ocean as a result of tidal flow over topographic features (e.g., Knight Inlet sill); internal hydraulic jumps can occur in lakes.

Progressive jumps form when supercritical flow (resulting from a gravity current, inflow, wind event or thermocline jet) propagates into an undisturbed region. Flow over a topographic feature can lead to a stationary jump in the lee of the obstacle. Localized energy dissipation and mixing occur near jumps and waves radiate from the critical point where $Fr = 1$. The impacts and distribution of hydraulic phenomena in lakes are not well understood.

Regime 2: Solitary Waves

In small- to medium-sized lakes subjected to moderate forcing ($0.3 < W^{-1} < 1.0$), nonlinearities become significant and the linear wave equation no longer completely describes wave evolution. In addition to the linear standing wave (composed of symmetric cosine components combined in a standing wave pattern), asymmetrical nonlinear wave components are generated from the wind induced thermocline tilt. The asymmetric components combine into a progressive internal wave pattern. The downwelled fluid becomes a dispersive packet of sub-basin scale internal waves of depression (Figure 10) called nonlinear internal waves (NLIWs), while upwelled fluid evolves into a progressive nonlinear basin-scale wave, referred to as a rarefaction or internal surge.

The weakly nonlinear Korteweg-de-Vries (KdV) equation mathematically describes the generation and unidirectional progression of NLIW from the wind-induced thermocline setup

$$\frac{\partial \eta}{\partial t} + c_o \frac{\partial \eta}{\partial x} + \alpha\eta \frac{\partial \eta}{\partial x} + \beta\eta \frac{\partial^3 \eta}{\partial x^3} = 0$$

where the nonlinear coefficient $\alpha = (3c_o/2)(h_1 - h_2)/h_1h_2$ and the dispersive coefficient $\beta = c_o h_1 h_2/6$. Initially, the internal surge propagates under a balance between the unsteady $(\partial\eta/\partial t)$ and nonlinear $\alpha\eta(\partial\eta/\partial x)$ terms. As nonlinearities become more apparent as the waveform steepens and the wavefront approaches vertical (Figure 10c). This occurs at the steepening time scale

$$T_s = \frac{L}{\alpha\delta\eta}$$

Wave steepening causes the dispersive term $\beta\eta(\partial^3\eta/\partial x^3)$ to become significant, eventually balancing nonlinear steepening at $t = T_s$, leading to the production of high-frequency NLIWs (Figure 10d).

In many lakes, NLIWs have a wave profile that matches a particular solution to the KdV equation

$$\eta(x,t) = a\,\mathrm{sech}^2\left(\frac{x - ct}{\lambda}\right)$$

These are called solitary waves. The maximum amplitude of the solitary wave a, the solitary wave speed c, and characteristic horizontal length-scale λ are given by

$$c = c_o + \frac{1}{3}\alpha a \text{ and } \lambda^2 = 12\frac{\beta}{a\alpha}$$

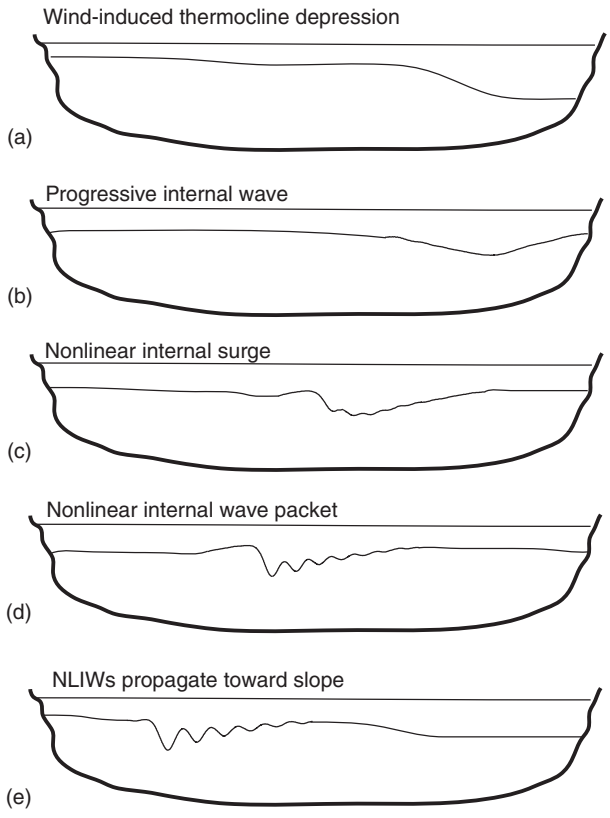

Figure 10 Schematic showing the evolution of a NLIW packet. (a) Initial wind induced thermocline depression, (b–c) formation of a progressive surge through nonlinear steepening, (d–e) evolution of a dispersive NLIW packet at $t = T_s$. For the case shown, the wind had been blowing for less than $T_1/4$ and a steady state tilt of the entire thermocline was not achieved (i.e., upwelling did not occur). This is a common occurrence in long (~100 km) narrow lakes (e.g., Seneca Lake, Babine Lake, etc.).

The KdV equation reveals some interesting characteristics of solitary waves. In a two-layer system they will always protrude into the thicker layer and so are generally observed as waves of depression upon the thermocline. If the interface occurs at mid-depth, $\alpha \to 0$; thus preventing nonlinear steepening and subsequent solitary wave generation. Moreover, the dependence of α on $h_1 - h_2$ demonstrates that the degree of nonlinearity depends not only on the magnitude of the interfacial displacement, but also on the relative heights of the stratifying layers.

The dispersive nature of the wave packet is evident from the relationship between wave amplitude a and wave speed c; a spectrum of waves in a particular packet will be rank ordered according to amplitude (Figure 10e) and will disperse with time as they propagate. An estimate of the number of solitary waves and their amplitudes, while beyond the scope of this article, may be obtained from the Schrödinger wave equation.

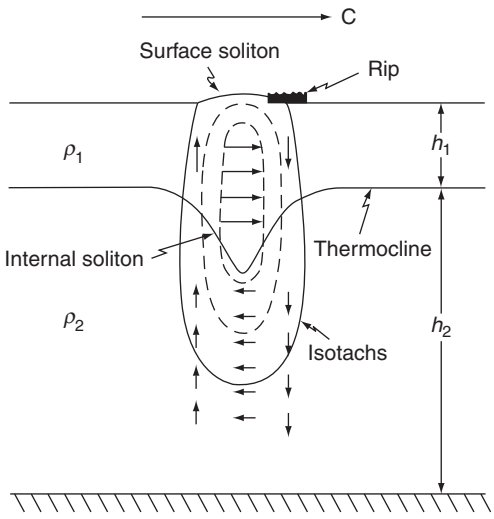

Figure 11 Schematic showing the passage of an internal solitary wave in a two-layer stratified fluid. Dashed lines are contours of water particle speed (isotachs) and arrows indicate the magnitude and direction of the flow. A small surface solitary wave of amplitude $\sim (\rho_2 - \rho_1)a$ accompanies the solitary wave and causes the rip or surface slick. From Osborne AR and Burch TL (1980) Internal solitons in the Andaman Sea. *Science* 208 (4443): 451–460.

Laboratory experiments show that NLIWs can contain as much as 25% of the energy (APE) introduced to the internal wave field by the winds. In large lakes they may have amplitudes and wavelengths as large as ~20 m and ~50–1000 m, respectively, and travel at $c \sim 0.5$–$0.75\ \mathrm{ms}^{-1}$. The velocity field associated with large amplitude NLIWs, commonly found in the ocean, will form a slick (rip) on the water surface (Figure 11) allowing them to be located and tracked using shore-based, aerial or satellite imagery.

Shoaling of Nonlinear Internal Waves

Progressive nonlinear internal waves travelling along the thermocline will break when they shoal upon the sloping lake bottom (Figure 12). Wave breaking irreversibly converts wave energy to mixing and dissipation, thus contributing to localized intense turbulence in the TBBL. The internal breaking process is similar to surface wave breaking at a beach and may be interpreted in the same manner using an internal form of the Iribarren number form of the Iribarren number ξ, which is the ratio of the boundary slope(s) to the offshore wave slope (a/λ)

$$\xi = \frac{s}{(a/\lambda)^{1/2}}$$

The relationship between ξ and the breaking mechanism is an ongoing area of active research. Laboratory experiments show that for small ξ (Figure 13(a)),

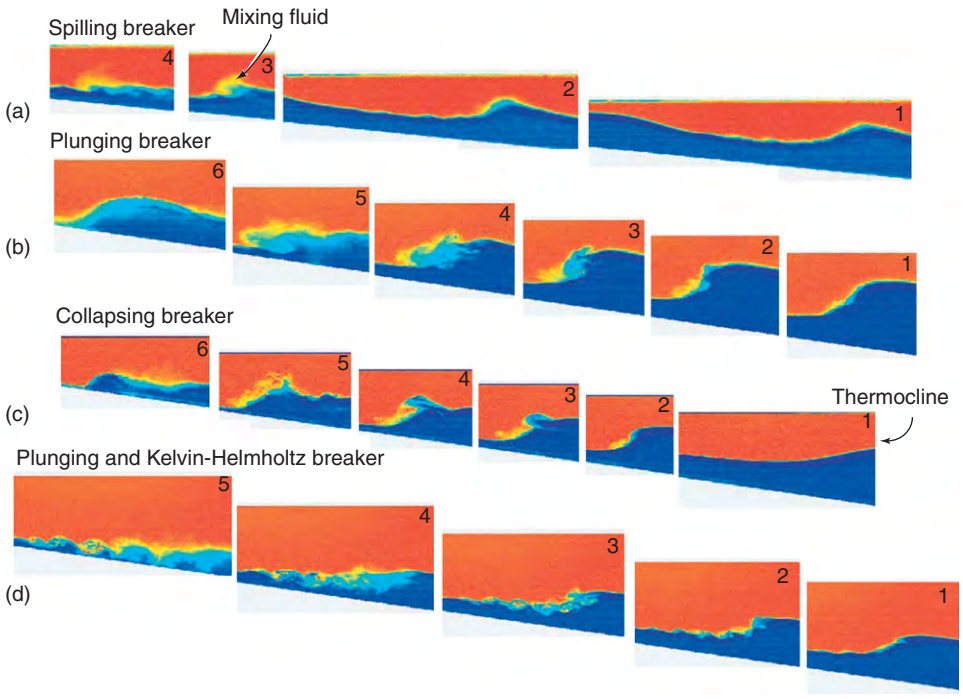

Figure 12 False color images showing types of internal wave breakers: (a) spilling breakers, (b) plunging and (c) collapsing breakers, (d) mixed plunging and Kelvin–Helmholtz breaking. Note the steepening of the rear face of the incident wave of depression, the transformation to a wave of elevation and subsequent breaking. Small numbered figures denote different stages of the breaking process. Adapted from Boegman L, Ivey GN, and Imberger J (2005) The degeneration of internal waves in lakes with sloping topography. *Limnology and Oceanography* 50: 1620–1637.

spilling breakers occur when small-scale shear instabilities form on the wave crests prior to breaking, causing mixing to be suppressed by viscosity. The mixing efficiency $R_f = b/(b+\epsilon)$, where b is the energy lost irreversibly to mixing and ε the energy dissipated by viscosity as heat, is less than 15%. As ξ increases, plunging (Figure 12(b)) then collapsing (Figure 12(c)) breakers occur. In the plunging region, wave inertia dominates and the most energetic overturns approach the Ozmidov scale (the largest scale where inertia can overcome buoyancy); the potential energy available for mixing is maximized and $R_f > 15\%$. For collapsing breakers, the wave breaking processes is not sufficiently energetic to overcome the stratification, mixing is suppressed by buoyancy and $<R_f$ 15%. For $\xi \to 1$ surging breakers occur, $R_f \to 0$ and the wave energy is reflected from the slope. Mixed-mode convective and shear-driven breaking is also possible when the wave shoals through a strong background flow field (Figure 12(d)).

Progressive Internal Wave Rays in a Continuous Stratification

We have conveniently described standing waves in a continuous stratification in terms of wave modes. A continuous stratification will also support progressive sub-basin scale internal waves; however, it is more insightful to describe these waves in terms of rays (both methods of analysis can be shown to be equivalent). Unlike NLIWs, which require a thermocline waveguide, progressive waves in a continuous stratification are described by linear equations and occur in regions of the water column where $N > 0$ and slowly varying (e.g., Figure 1(e,f)). A disturbance in the flow (e.g., flow over rough topography) with a particular excitation frequency will generate a range of wavelengths that will radiate from the source at the same frequency. The wave rays will propagate through the fluid at a fixed angle to the horizontal β given by the dispersion relation

$$\omega = N \sin\beta = \frac{kN}{K}$$

where ω is the wave frequency and the wavenumber vector $K = \sqrt{k^2 + m^2}$ has horizontal k and vertical m components (Figure 13(b)). The angle at which the rays propagate is chosen such that the vertical component of their frequency matches N, leading to a four-ray St. Andrew's cross pattern (Figure 13(a)). From the dispersion relation, the wave frequency is independent of the magnitude of the wavelength and only depends upon β. This property is quite different than for interfacial waves, where the wave frequency and period depend only on the magnitude of the wavelength.

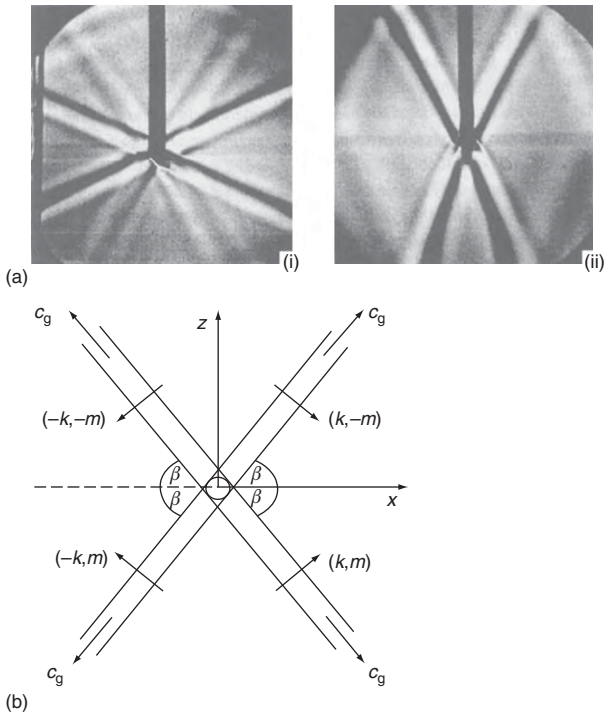

Figure 13 Propagation of internal wave rays in a stratified fluid with constant *N*. (a) Laboratory images showing internal wave rays propagation from an oscillating cylinder. The light and dark bands are lines of constant phase (wave crests and troughs). In (i) and (ii) $\omega = 0.4N$ and $0.9N$ giving $\beta = 25°$ and 64°, respectively. From Mowbray DE and Rarity BSH (1967) A theoretical and experimental investigation of the phase configuration of internal waves of small amplitude in a density stratified liquid. *Journal of Fluid Mechanics* 28: 1–16. (b) Schematic showing the direction of the group velocity c_g, wavenumber vectors (showing the direction of phase propagation), and angle of inclination of the rays relative to the horizontal β, for the experiments in (a). Adapted from Thorpe SA (2005) *The Turbulent Ocean*. Cambridge, UK: Cambridge University Press.

Equations for the velocity and density perturbations induced by the wave passage are beyond the scope of this review and can be found in physical oceanography texts.

Another property of the dispersion relation is that the wave frequency must lie in the range $0 < \omega < N$, mathematically showing that N is indeed the cut-off frequency for internal waves. Excitation at frequencies $\omega > N$ generates motions that are exponentially damped. Wave energy will propagate from an excitation region at the group velocity c_g of the wave envelope, which is perpendicular to the phase velocity c; the wave rays carry the energy at right angles to the motion of the crests and troughs! These waves are difficult to visualize, internal waves generated by a local source do not have the concentric circle pattern of crests and troughs familiar to those who observe a stone thrown into a pond, but are composed of crests that stretch outward as spokes (rays) carrying energy radially from the source. The wave crests and troughs slide perpendicularly across the rays, seeming to appear from and disappear to nowhere.

From the discussion above, it is not surprising that internal wave rays do interesting things as they reflect from sloping topography and propagate into regions of variable $N(z)$. The intrinsic frequency ω is always conserved causing rays propagating into depths of diminishing $N(z)$ to refract towards the vertical and be totally reflected at the turning depth where $\omega = N(z)$. If generated in the seasonal thermocline these waves can be trapped between the upper and lower surfaces of the metalimnion where $\omega < N(z)$. Waves propagating into depths of increasing $N(z)$, such as toward the seasonal thermocline, will refract toward the horizontal.

Upon reflection from the lake surface or a sloping bottom with angle α, the intrinsic wave frequency is conserved and, by the dispersion relation, the reflected ray must propagate at the same angle β as the incident ray (**Figure 14**). The wavelength and group velocity will change as is evident in the change in concentration of wave rays upon refection. If $\alpha = \beta$, the rays are reflected parallel to the slope and have zero wavelength and group velocity. A turbulent bore will from and propagate along the slope and wave energy is rapidly converted into local dissipation and mixing. In this case, both the slope angle and wave frequency are considered critical.

Subcritical waves $\beta < \alpha$ will be reflected back in the direction from which they came and the may escape to deeper water (**Figure 14(c,d)**). However, supercritical waves $\beta > \alpha$ will continue in the same direction (**Figure 14(a)**) and if propagating towards shallower water in the littoral zone may thus be trapped, repeatedly reflecting off the surface, lakebed and turning depths (**Figure 15**). Eventually the rays will break when on a critical slope $\alpha = \beta$, where they have a critical frequency $\omega = N \sin \alpha$.

Progressive internal waves are produced by small localized disturbances such as flow over rough topography, patches of shear and turbulence and wave-wave/wave-flow interactions, when the excitation frequency $\omega < N$. Progressive waves are found ubiquitously in lakes and those in the 10^{-5} to 10^{-3} Hz bandwidth generally have critical frequencies relative to the sloping boundaries found where the metalimnion intersects the lake bed.

Resonant and Forced Internal Waves

The periodicity inherent in weather patterns creates over-lake wind fields that occur at regular frequencies. For example, the winds over Lake Erie have

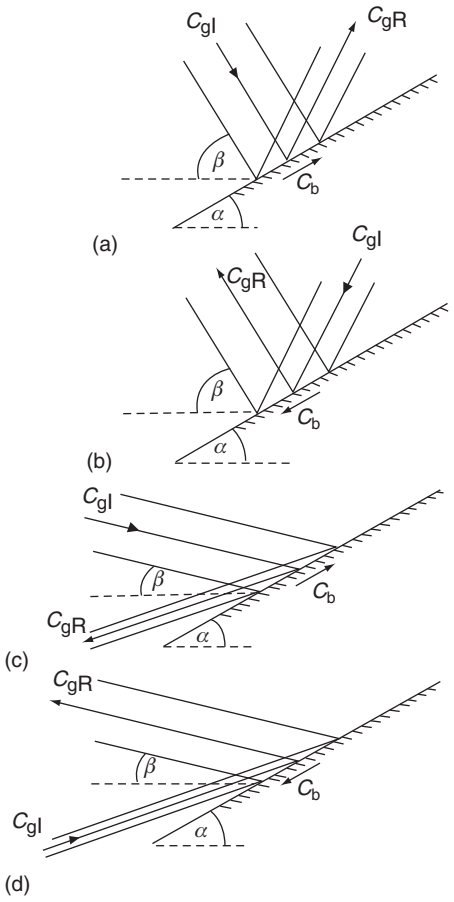

Figure 14 Schematic showing the reflection of internal wave rays from a uniform slope. The lines indicate crests and troughs (lines of constant phase) and c_{gI} and c_{gR} the direction of the incident and reflected group velocity, respectively; c_b is the direction of phase propagation on the slope. (a–b) show the supercritical case where $\alpha < \beta$ and rays continue upslope or downslope. (c–d) show the subctitical case $\alpha > \beta$ where rays are reflected out to deeper water. The distance between rays is proportional to the wavelength and can increase or decrease upon reflection. As $\beta \rightarrow \alpha$, the reflected rays become parallel to the slope and their wavelength goes to zero. Adapted from Thorpe SA and Umlauf L (2002) Internal gravity wave frequencies and wavenumbers from single point measurements over a slope. *Journal of Marine Research* 60: 690–723.

periodicities of 10 d and 24 h, associated with frontal weather systems and diurnal land/sea breeze phenomena, respectively. When the forcing frequency matches one of the natural frequencies of the basin-scale wave modes, resonant amplification will occur. Seasonal heating and deepening of the thermocline will adjust the natural frequencies relative to the forcing frequencies, thus tuning the system into and out of resonance.

Laboratory experiments show that the relative frequencies of the wind forcing f_w and H1 internal seiche f_{H1} can be used to model internal wave response to periodic forcing conditions (Figure 16). When the forcing frequency of the wind stress is less than the natural frequency of the H1 internal seiche ($f_w < \sim 2/3 f_{H1}$), the phase of the basin-scale oscillations are reset with each wind event and a forced internal seiche is generated at the same frequency as the wind forcing. A resonant H1 seiche will occur when the frequency of the wind forcing is near the frequency of the H1 seiche ($2/3 f_{H1} < f_w < 2 f_{H1}$) and when the forcing frequency is greater than the natural frequency of the H1 seiche ($f_w > \sim 2 f_{H1}$), higher-mode horizontal seiches are generated. Resonance appears to be particularly effective in amplifying the response of the second vertical mode (e.g., Lake Alpnach) and the even horizontal modes that are not naturally energized by a wind-induced interfacial setup.

Resonance between the wind and the H1 internal mode leads to increased seiche amplitudes under relatively weak wind forcing conditions. For example, when $W^{-1} > 0.03$, nonlinearities become significant (compared to $W^{-1} > 0.3$ under non-resonant conditions), favoring the formation of steepened internal wave fronts (e.g., Loch Ness) and progressive NLIWs. If the wind induced tilting increases, $W^{-1} > 0.2$ will cause Kelvin–Helmholtz instabilities to form within the progressive NLIWs, leading to significant diapycnal mixing within the basin interior. The energy content of the H1 seiche, NLIWs and shear instability modes thus appear to be capped and continued energy input via resonant amplification is transferred between these discrete modes, ultimately being lost to dissipation and mixing at turbulent scales.

Analysis of Timeseries Data

The various wave, instability and turbulence processes described in this chapter are shown schematically in Figure 17. These processes occur beneath the lake surface and so practicing limnologists do not have the luxury of being able to directly observe them in the field. Some insight regarding their spatial structure is gained from idealized laboratory and computational models (see **Hydrodynamical Modeling**) but for the most part, limnologists must resort to deciphering timeseries data from thermistor chains, which are the most useful tools in their arsenal. Figure 18 shows many of the processes from Figure 17 as they would appear on thermistor data, which has been contoured to show isotherm displacement timeseries with depth.

During the strong wind event, shear instabilities form at the base of the surface layer (Figure 18(d)). Shortly thereafter, a thermocline jet occurs within a compressed region of the metalimnion and causes a rapid expansion of the strata and localized mixing

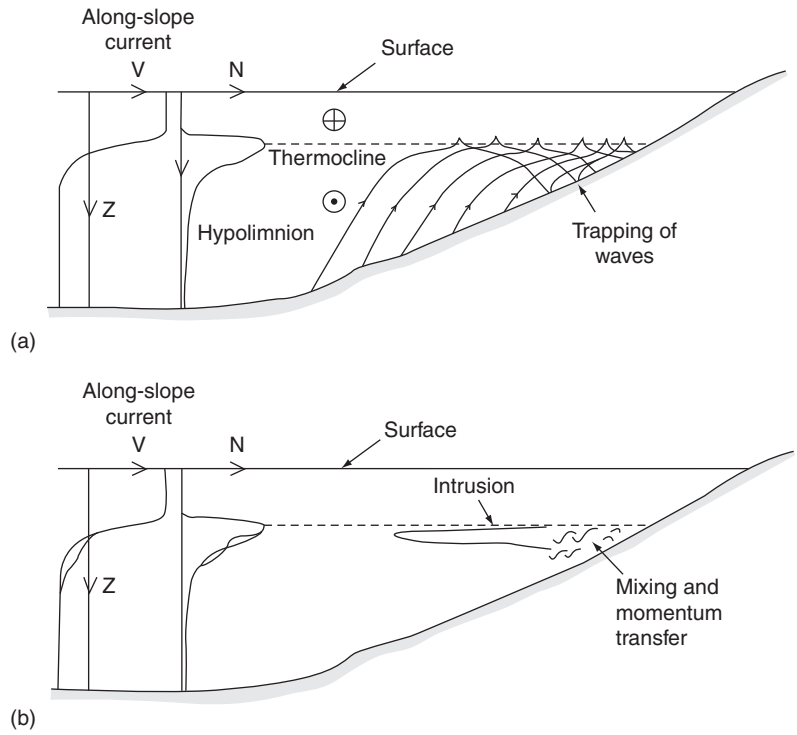

Figure 15 Schematic showing wave rays radiating from along-slope flow over bottom topography and propagating toward the littoral zone. (a) The waves are trapped between the mixed surface layer and the lake bed and will eventually break where the bed slope α is critical and the wave frequency $\omega = N\sin\alpha$. (b) The mixed fluid created during wave breaking collapses and intrudes into the lake interior, carrying sediment and nutrients from the littoral zone. The local strength of the stratification N' is reduced and the along-slope flow is modified. Adapted From Thorpe SA (1998). Some dynamical effects of internal waves and the sloping sides of lakes. Coastal and estuarine studies: Physical processes in lakes and oceans. *American Geophysical Union* 54: 441–460.

(Figure 18(e)). The basin-scale internal wave energized by the wind event has steepened into an internal surge supporting large amplitude NLIWs of depression and series of step like features resembling internal hydraulic jumps (Figure 18(c)). The surge wave interacts with the lake bed leading to significant mixing over the bottom 20 m of the water column.

The motions described above all result from a single intense wind event. Considering the periodic nature of surface winds, it is not surprising that periodic wave motions occur in lakes over a range of length scales and frequencies. Spectral frequency analysis is used to conveniently analyze timeseries data and determine the relative amount of energy found at each frequency.

Observations from many lakes suggest the existence of a universal frequency spectrum model for lakes. The main features of the internal wave spectrum are shown for several lakes in Figure 19. These lakes range in diameter from 20 km (Lake Biwa) to 10 km (Lake Kinneret) to 1 km (Lake Pusiano). Unlike the spectral energy cascade occurring in turbulent flows, internal waves are generated at discrete frequencies throughout the spectrum. Motions are bounded at the low frequency end of the spectrum by H1 seiches that contain the most energy with frequencies between zero and 10^{-4} Hz. At the high-frequency end of the spectrum, motions are bounded by the high-frequency cut-off N. Shear instabilities cause a sub-N spectral peak with frequency $\sim 10^{-2}$ Hz and five orders of magnitude less energy than the basin-scale seiches. The middle portion of the spectrum contains freely propagating linear and nonlinear internal waves. The NLIWs are generated under moderate forcing conditions with sech^2 or solitary wave profiles and frequencies $\sim 10^{-3}$ Hz. These waves are short lived because they break upon shoaling topography at the depth of the thermocline. The portion of the spectrum between the basin-scale seiches and NLIWs (i.e., $\sim 10^{-4}$ Hz) appears to consist of freely propagating gravity waves that have linear or sinusoidal profiles; similar to the broadband background internal wave field associated with the Garrett-Munk spectrum in the ocean. These waves are generated by disturbances within the flow field (radiation from flow over rough topography, wave–wave interactions, mixing regions, intrusions, nonlinear surges and internal hydraulic jumps) where gravity acts as

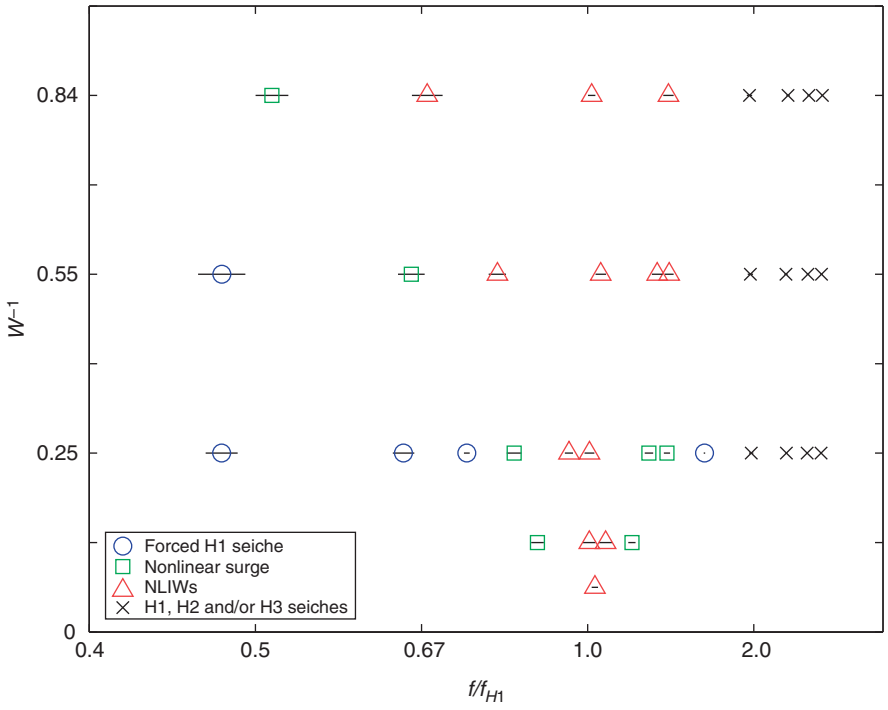

Figure 16 Regime diagram showing the dominant internal wave response under periodic forcing conditions in a long rectangular laboratory tank. Error bars denote the variation in forcing during an experiment (mean ± standard deviation). After Boegman L and Ivey GN (2007) Experiments on internal wave resonance in periodically forced lakes. In *Proceedings of the 5th International Symposium on Environmental Hydraulics*, 4–7 Dec. 2007, Tempe, Arizona.

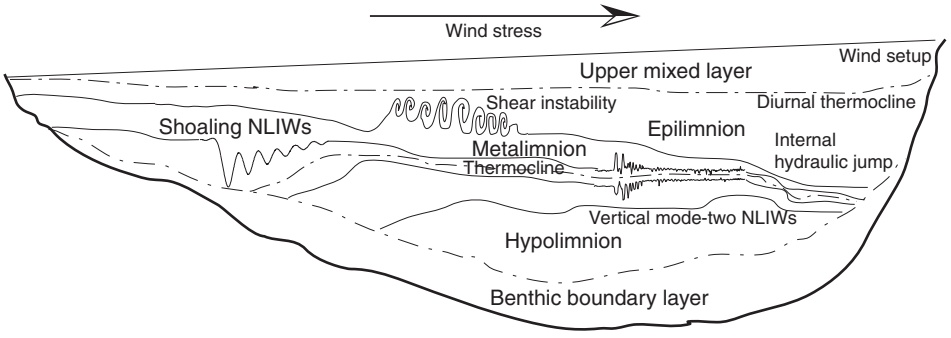

Figure 17 Pictorial representation of the various regions of a lake and some of the wave-like physical processes that occur. See also **Figure 6.13** in Fischer HB, List, EJ, Koh RCY, Imberger J, and Brooks NH (1979) *Mixing in Inland and Coastal Waters*. San Diego, CA: Academic Press; **Figure 15** in Imberger J (1985) Thermal characteristics of standing waters: An illustration of dynamic processes. *Hydrobiologia* 125: 7–29; and **Figure 7** in Imboden DM and Wüest A (1995). Mixing mechanisms in lakes. In Lerman A, Imboden DM, and Gat J (eds.) *Physics and Chemistry of Lakes.* pp. 83–138. Berlin: Springer.

restoring force on fluid parcels displaced from their equilibrium position. The waves in this frequency bandwidth are interacting with one another making it difficult to identify their source. The bandwidth limits on the spectrum depend only upon the stratification and basin size and are independent of the strength of the wind forcing. Stronger winds lead to sharper energy peaks with higher energy content (larger amplitude seiches and more shear instabilities).

Summary

The dynamical interplay between stratification, waves, and wind can is best summed up in using the conceptual model proposed by J. Imberger in 1990 and supported by the more recent measurements by A. Wüest and others. A lake behaves like an engine that is powered by the wind and does work against the potential energy gradient embodied in the stratification. Approximately 2% of the wind energy flux

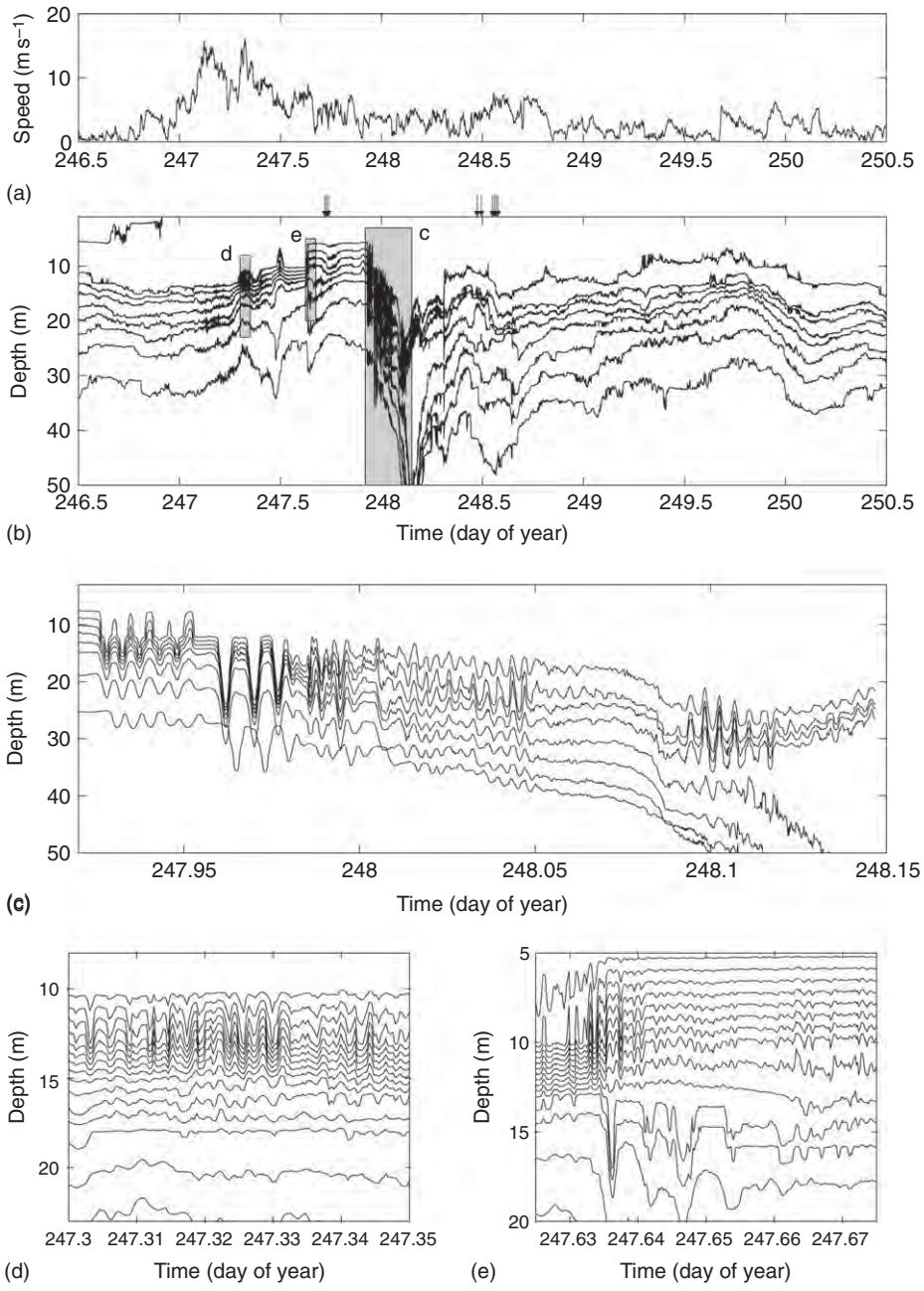

Figure 18 Observations from Lake Biwa (Japan) in 1993 showing steepened nonlinear basin-scale internal wave front and associated nonlinear internal waves. (a) Wind speed collected at 10-min intervals showing the passage of a storm event; (b) nonlinear response of basin-scale internal wave field showing steepened wave front (2 °C isotherms); (c) magnified view of shaded region in panel b showing details of NLIWs (2 °C isotherms). (d) Magnified view of shaded region d in panel b showing shear instabilities resulting from enhanced shear at the base of the surface layer during the strong wind event (1 °C isotherms); (e) Magnified view of shaded region e in panel b showing a V2 expansion of the metalimnion resulting from a thermocline jet that forms after a period of metalimnion compression (1 °C isotherms). The bottom isotherm in panels b and c is 10 °C. Adapted from Boegman L, Imberger J, Ivey GN, and Antenucci JP (2003). High-frequency internal waves in large stratified lakes. *Limnology and Oceanography* 48: 895–919.

enters the lake; of this ~80% is dissipated in the surface layer and ~20% is transferred to the basin-scale internal wave field. The basin-scale seiches energized by the wind are frictionally damped as they swash along the lake bed and by degeneration into progressive high-frequency internal waves, shear instabilities, and eventually turbulence. Approximately 90% of the seiche energy is lost energizing turbulent dissipation and mixing in the TBBL; <1/4 of which first passes through the nonlinear internal

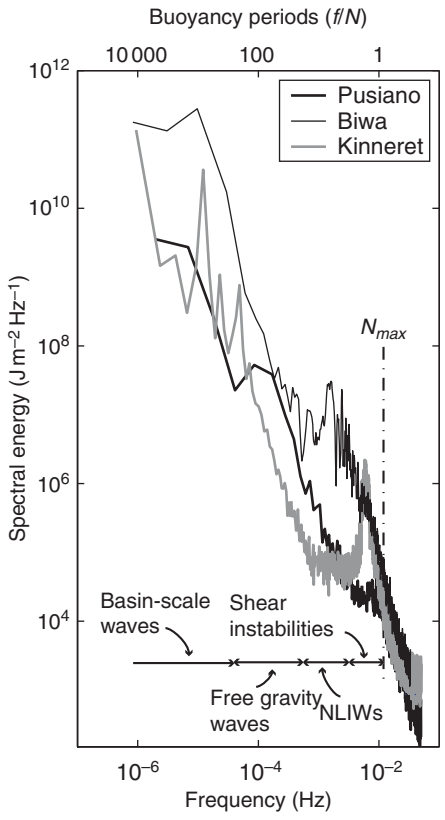

Figure 19 Spectra of the vertically integrated potential energy signals from Lakes Pusiano, Kinneret and Biwa showing basin-scale seiches (0–10^{-4} Hz), freely propagating nonlinear wave groups with sinusoidal profiles ($\sim 10^{-4}$ Hz) and solitary wave profiles ($\sim 10^{-3}$ Hz), and shear instabilities ($\sim 10^{-2}$ Hz). N_{max} denotes the maximum buoyancy frequency. Adapted from Boegman L, Ivey GN, and Imberger J (2005). The degeneration of internal waves in lakes with sloping topography. *Limnology and Oceanography* 50: 1620–1637.

wave field prior to wave breaking and $> 3/4$ of which is lost to frictional swashing in the TBBL. The remaining ~10% of the seiche energy results in intermittent shear instability in the basin interior. The overall mixing efficiency of the turbulence is ~15% leading to an upwards buoyancy flux that works to weaken the stratification and raise the centre of gravity of the lake. The lake engine is extremely inefficient with only ~0.06% of the wind work acting to irreversibly mix the stratification; the bulk of the wind work is lost to frictional viscous dissipation, which due to the large heat capacity of water has no significant effect on the lake temperature. From this model, it is clear that while internal waves control biogeochemical mixing and transport within a stratified waterbody, they are not able to significantly influence the stratification upon which they propagate. Consequently, their existence depends entirely upon the seasonal stratification cycle set up by the surface thermodynamics.

See also: The Benthic Boundary Layer (in Rivers, Lakes and Reservoirs); Currents in Stratified Water Bodies 1: Density-Driven Flows; Currents in Stratified Water Bodies 3: Effects of Rotation; Currents in the Upper Mixed Layer and in Unstratified Water Bodies; Density Stratification and Stability; Hydrodynamical Modeling; Mixing Dynamics in Lakes Across Climatic Zones; Salinity; Small-scale Turbulence and Mixing: Energy Fluxes in Stratified Lakes; The Surface Mixed Layer in Lakes and Reservoirs.

Further Reading

Boegman L, Imberger J, Ivey GN, and Antenucci JP (2003) High-frequency internal waves in large stratified lakes. *Limnology and Oceanography* 48: 895–919.

Boegman L, Ivey GN, and Imberger J (2005) The degeneration of internal waves in lakes with sloping topography. *Limnology and Oceanography* 50: 1620–1637.

Fischer HB, List EJ, Koh RCY, Imberger J, and Brooks NH (1979) *Mixing in Inland and Coastal Waters*. San Diego, CA: Academic Press.

Helfrich KR and Melville WK (2006) Long nonlinear internal waves. *Annual Review of Fluid Mechanics* 38: 395–425.

Horn DA, Imberger J, and Ivey GN (2001) The degeneration of large-scale interfacial gravity waves in lakes. *Journal of Fluid Mechanics* 434: 181–207.

Imberger J (1998) Flux paths in a stratified lake: A review. Coastal and estuarine studies: Physical processes in lakes and oceans. *American Geophysical Union* 54: 1–18.

Imberger J and Patterson JC (1990) Physical limnology. *Advances in Applied Mechanics* 27: 303–475.

Imboden DM and Wüest A (1995) Mixing mechanisms in lakes. In: Lerman A, Imboden DM, and Gat J (eds.) *Physics and Chemistry of Lakes*, pp. 83–138. Berlin: Springer.

Lazerte BD (1980) The dominating higher order vertical modes of the internal seiche in a small lake. *Limnology and Oceanography* 25: 846–854.

MacIntyre S, Flynn KM, Jellison R, and Romero JR (1999) Boundary mixing and nutrient fluxes in Mono Lake, California. *Limnology and Oceanography* 44: 128–156.

Mortimer CH (1974) Lake hydrodynamics. *Mitteilungen Internationale Vereinigung Limnologie* 20: 124–197.

Mortimer CH (2004) *Lake Michigan in Motion*. 310 pp. Madison: The University of Wisconsin Press.

Münnich M, Wüest A, and Imboden DM (1992) Observations of the second vertical mode of the internal seiche in an alpine lake. *Limnology and Oceanography* 37: 1705–1719.

Thorpe SA (1998) Some dynamical effects of internal waves and the sloping sides of lakes. Coastal and estuarine studies: Physical processes in lakes and oceans. *American Geophysical Union* 54: 441–460.

Thorpe SA (2005) *The Turbulent Ocean*. Cambridge, UK: Cambridge University Press.

Turner JS (1973) *Buoyancy Effects in Fluids*. Cambridge, UK: Cambridge University Press.

Wüest AJ and Farmer DM (2003) Seiches. *McGraw-Hill Encyclopedia of Science and Technology*, 9th ed. New York: McGraw-Hill.

Wüest A and Lorke A (2003) Small-scale hydrodynamics in lakes. *Annual Review of Fluid Mechanics* 35: 373–412.

Wüest A, Piepke G, and Van Senden DC (2000) Turbulent kinetic energy balance as a tool for estimating vertical diffusivity in wind-forced stratified waters. *Limnology and Oceanography* 45: 1388–1400.